JACS
JOURNAL OF THE AMERICAN CHEMICAL SOCIETY

Article

pubs.acs.org/JACS

Tricking a Protein To Swap Strands

Huabing Wang,[‡] Lisa Lang,[‡] Derek T. Logan,[†] Jens Danielsson,[‡] and Mikael Oliveberg*[,‡]

[‡]Arrhenius Laboratories of Natural Sciences, Department of Biochemistry and Biophysics, Stockholm University, 106 91 Stockholm, Sweden

[†]Division of Biochemistry and Structural Biology, Department of Chemistry, Lund University, Box 124, 221 00 Lund, Sweden

Supporting Information

ABSTRACT: Despite continuing interest in partly unfolded proteins as precursors for aggregation and adverse gain-of-function in human disease, there is yet little known about the local transitions of native structures that possibly lead to such intermediate states. To target this problem, we present here a protein-design strategy that allows real-time detection of rupture and swapping of complete secondary-structure elements in globular proteins—molecular events that have previously been inaccessible experimental analysis. The approach is applied to the dynamic β-barrel of SOD1, associated with pathologic aggregation in the neurodegenerative disease ALS. Data show that rupture and re-insertion of individual β-strands do not take place locally but require the SOD1 barrel to unfold globally. The finding questions the very existence of partly unfolded intermediates in the SOD1 aggregation process and presents new clues to the mechanism by which hydrogen bonding maintains global structural integrity.

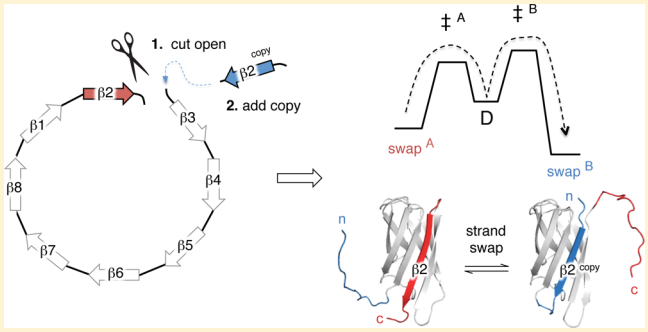

INTRODUCTION

The behavior of proteins is rarely apparent from static structures alone but hides in the elusive repertoire of conformational motions and environmental crosstalk. Pressing examples are the conspicuous tuning of protein stability in live cells,[1,2] the yet poorly understood mechanisms of quinary protein organization,[3] and the long-standing question about how pathologic protein aggregation actually initiates and spreads.[4−7] Considerable progress in identifying the intermediates and structural dynamics of these processes has come from relaxation−dispersion NMR[8] and H−D exchange analysis,[9] revealing at atomistic detail which regions of the proteins are susceptible to structural changes and intermolecular interactions.[10] Also, information about how proteins ultimately rupture completely has been inferred from phi-value analysis,[11] presenting snapshots of protein structures at the transition state to global disorder.[12,13] For scientists who try to use these results for pinning down the repertoire of possible structural motions, however, there are two immediate shortcomings. First, the available data only cover events at the lower and highest ends of the reaction free-energy profiles, leaving the middle region blank (Figure 1): relaxation−dispersion NMR (CPMG) detects states with population of >0.5%,[8] H−D exchange sees only states more stable than the globally unfolded ensemble,[13] and phi-value analysis targets selectively the barrier maxima.[11] Second, since the measurements are ensemble averages, it is often not clear to what extent the data represent contiguous unfolding of local structural elements, i.e., complete β strands or α helices,[9] or merely diffuse breathing within elements that remain embedded in their native context.[10] Accordingly, conventional analysis will not suffice to shed light on the question we ask here, namely, how tightly does a β-barrel protein hold on to its strands during native-state fluctuations? This question is important not only for delineating secondary-structure plasticity in biological function but also for mapping out possible misfolding and aggregation pathways. To resolve the problem, we present here an alternative strategy to follow—in real time—how individual β-strands dislodge and swap with one another in the folded state (Figure 2). In essence, the approach is based on inserting two identical copies of the target β-strand in the protein sequence and allowing structural competition and dynamic exchange to occur (Figure 2). Our protein model is the monomeric β-barrel of the amyotrophic lateral sclerosis (ALS)-associated protein Cu/Zn superoxide dismutase (SOD1), constructed by truncation of the functional loops[14] ($SOD1^{barrel}$). The advantage of the SOD1 model system is that it is already comprehensively benchmarked with respect to (i) X-ray/NMR structures,[10] (ii) conformational dynamics[14] and allosteric motions,[15] (iii) folding pathway[16] and functional frustration,[17] (iv) *in vitro*/*in vivo* aggregation mechanism,[7] (v) fibrillar structure,[18,19] and (vi) *in-cell* stability,[1] providing extensive constraints for mechanistic interpretation and experimental design. The strand-swap analysis shows that $SOD1^{barrel}$ is remarkably robust and does not allow individual β-strands to dislodge and swap unless the protein is completely unfolded and refolded back again. Our conclusion is thus that the hydrogen bonding of SOD1 remains at some level intact through even the most extreme native-state fluctuations, providing further clues to the

Received: May 19, 2016
Published: October 26, 2016

DOI: 10.1021/jacs.6b05151
J. Am. Chem. Soc. 2016, 138, 15571−15579

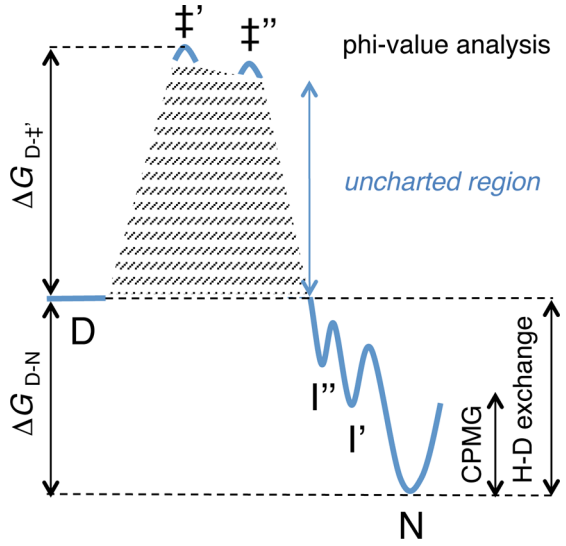

Figure 1. Schematic folding free-energy profile (D → N) of a globular protein. Structural information about the maxima is obtained by transition-state analysis (‡′ and ‡″), and information about the lower regions by H−D exchange and CPMG NMR analysis (I′ and I″). As the latter approaches are inherently limited to free energies below D, this leaves the middle region of the native basin inaccessible to conventional experimental analysis. For details of the ‡′, ‡″ and I′, I″ structures of the SOD1^{barrel}, see Figure 6.

structural properties and erroneous side reactions of β-barrel proteins.

RESULTS

Experimental Rationale. For simplicity, we start by assuming the SOD1^{barrel} structure to be fully circularized; i.e., the backbone is linked into a ring (Figure 2). Any individual strand, for instance β2, can now be "peeled off" the central barrel by cutting it free at its c-terminal end, i.e., toward β3. The vacant barrel slot is then refilled with a second copy of β2 ($\beta2^{copy}$) that is linked up with β3 (Figure 2). By design, we are left with a frustrated protein construct (swap$^{\beta2}$) that can either remain folded with $\beta2^{copy}$ in the barrel position or swap back to the original β2 (Figure 2). Conversely, since swap$^{\beta2}$ has identical copies of β2 at either end of its primary sequence, the protein can choose one or the other when folding from the globally unfolded state. The outcome of this β-strand competition depends on the detailed features of the protein's free-energy profile, including those of the uncharted regions of the unfolding barrier (Figure 1). Following the design of swap$^{\beta2}$, we produced a series of strand-swap constructs to probe all parts of the SOD1 barrel as described below.

Outline of Strand-Swap Constructs, Reference Structures, and Nomenclature. To strictly map out the strand-swap events, we need first to benchmark the X-ray structures, stabilities, and folding behavior of all species involved. Sticking to the example in Figure 2, the two folded ground states of swap$^{\beta2}$ are structurally represented by the "parent" circular permutants P$^{2/3}$ (PDB 5J0C) and P$^{1/2}$ (PDB 5J07). We denote these competing states swap$^{\beta2}$/P$^{2/3}$ and swap$^{\beta2}$/P$^{1/2}$ (Figure 2). A difference between the swap$^{\beta2}$ ground states and the parent circular permutants is, however, that the former have one leftover β2-strand extending disordered from either the n- or c-termini (Figure 2). These disordered extensions modulate in some cases the folding and stability to a small extent. To account for such modulation, we extended the permutant termini—one residue at the time—while following the effects on the folding kinetics (Figure S1, Table S1). In the case of P$^{2/3}$, the n-terminal addition of AKESNG was sufficient to fully account for the extension effect, manifested in slight shifts of the refolding and unfolding rate constants (Supporting Information (SI)). This n-terminal adapted variant of P$^{2/3}$ was denoted P$^{2/3n}$ and used as reference for folding of swap$^{\beta2}$/P$^{2/3}$ (Table 1). As the disordered extension AKESNG involves only the loop between β2 and β3, it does not promote swap or otherwise alter the P$^{2/3n}$ structure, which remains identical to that of the original P$^{2/3}$ (SI). Corresponding extension to the c-terminus of P$^{1/2}$ shows no effect, allowing us to use this permutant as reference for the state swap$^{\beta2}$/P$^{1/2}$ without modification (Table 1). In cases where such c-terminal adaptation is required, we denote these with the superscript extension "c" (Table 1). Accordingly, the analysis of the β2 exchange behavior was based on the three constructs swap$^{\beta2}$, P$^{2/3n}$, and P$^{1/2}$ (Table 1). Following the same protocol and nomenclature, analogous triads of constructs were produced for the other target strands of the SOD1^{barrel} structure (Figures 3−4, Table 1, and SI).

Structural and Kinetic Characterization of the Permutant Reference States. The structures of the parent permutants P$^{1/2}$, P$^{2/3}$, P$^{4/5}$, P$^{7/8}$, and P$^{8/1}$ ≡ SOD1^{barrel} were determined by X-ray crystallography and used to infer the structures of the competing ground states of the strand-swap constructs in Figures 2−4. In summary, the X-ray data show that circular permutation has negligible impact on the SOD1^{barrel} structure, providing a stringent molecular base for the strand-swap analysis (Figure S2). The only permutant that failed to produce well-diffracting crystals was P$^{3/4}$. Next, the solution structures of the permutant references were verified by their HSQC NMR spectra (SI). The HSQC spectra are all very similar and consistent with X-ray data, showing that the solution structures of all proteins maintain the wild-type barrel architecture (Figure S3). The sole permutant without crystal structure, P$^{3/4}$, is highly unstable (Figure 2 and Table 1) and expected to consist of a mixture of folded and unfolded species at 0 M denaturant. Consistently, the P$^{3/4}$ spectrum shows double sets of HSQC cross-peaks, one that corresponds to the folded state and one to the unfolded state (Figure S3). The chemical shifts of the folded state cross-peaks verify that P$^{3/4}$ indeed has the same structure as the other permutant references (Figure S3). Finally, the stabilities and folding behavior of the parent permutants (P$^{1/2}$, P$^{2/3}$, P$^{3/4}$, P$^{4/5}$, P$^{7/8}$, and P$^{8/1}$) and the reference variants with adapted n- or c-termini (P$^{2/3n}$, P$^{2/3c}$, P$^{3/4n}$, P$^{4/5n}$, P$^{4/5c}$, P$^{7/8c}$, and P$^{8/1n}$, P$^{8/1c}$) were determined by standard chevron analysis[11] (SI) according to previous SOD1 protocols.[16] The results show that all permuted proteins maintain the archetypical two-state folding transition of the SOD1^{barrel} [14] (Figure 2, Table 1, and Figure S1). Also, the *m*-values and basic features of the chevron plots fall within the normal range of variation for circular permutation[20] and SOD1 point mutation.[16] Taken together, these data show that the folding free-energy profile of SOD1 is overall robust to changes in sequence connectivity.[12] When it comes to experimental identification, the references display clearly separated chevron plots (Figure 2), which enables kinetic analysis of the strand-swap events by conventional stopped-flow mixing and double-jump experiments.

Structural and Thermodynamic Comparison of the Strand-Swap Constructs and Their Permutant References. To confirm that the strand-swap constructs adopt the structures of their permutant references (Figures 2−4), the solution structures of swap$^{\beta2}$, swap$^{\beta3}$, swap$^{\beta8}$, swap$^{\beta1-4}$, and swap$^{\beta5-8}$ were verified by HSQC NMR at 0 M urea (SI). The "single-strand"

DOI: 10.1021/jacs.6b05151
J. Am. Chem. Soc. 2016, 138, 15571−15579

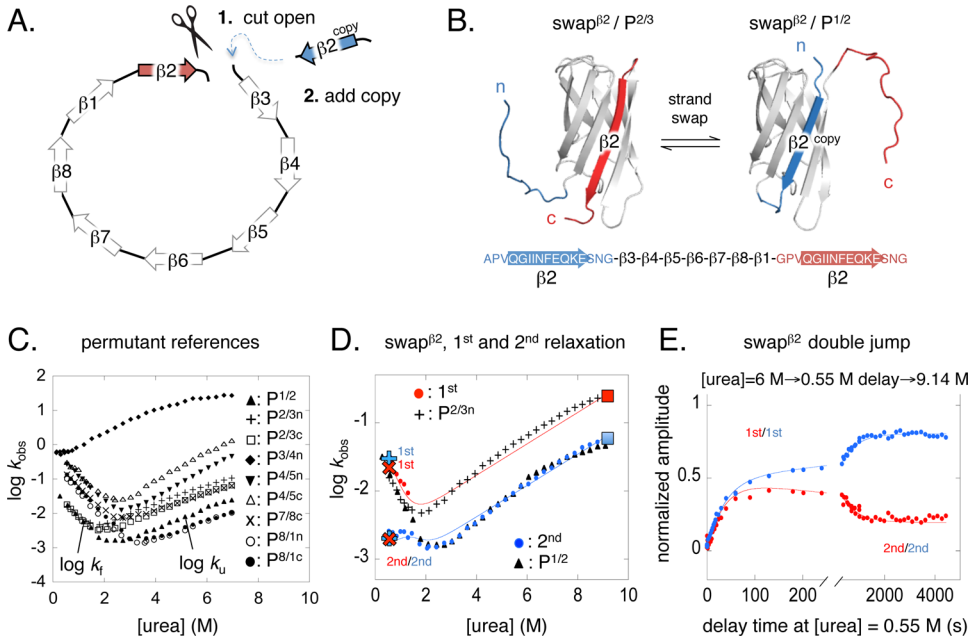

Figure 2. Strand-swap design and analysis. (A) The construct's n- and c-termini are first chosen by a single incision of the circularized SOD1 sequence, here between β2 (red) and β3 (white). Second, an extra copy of β2 (blue) is added to the n terminus. We denote this construct swap$^{\beta 2}$. (B) Swap$^{\beta 2}$ can now fold by recruiting either the red β2, attaining the structure swap$^{\beta 2}$/P$^{2/3}$, analogous to that of the circular permutant P$^{2/3}$ (PDB 5J0C), or the blue β2, attaining the structure swap$^{\beta 2}$/P$^{1/2}$, analogous to that of the circular permutant P$^{1/2}$ (PDB 5J07). The protein is also free to interconvert between the alternate states, swap$^{\beta 2}$/P$^{2/3}$ and swap$^{\beta 2}$/P$^{1/2}$, by swapping β2 segments. (C) Folding chevron plots of the various permutant proteins used as references in this study. As exemplified for P$^{2/3n}$, the left-hand limb of the plots shows the refolding rate constants (log k_f), and the right-hand limb the unfolding rate constants (log k_u). All references display archetypical two-state behavior (SI). The references for swap$^{\beta 2}$ are P$^{2/3n}$ and P$^{1/2}$, where the superscript "n" denotes n-terminal modification (Table S1). (D) The chevron plot of swap$^{\beta 2}$ displays two relaxation phases (first and second), overall matching the chevron plots of the permutant references P$^{2/3n}$ and P$^{1/2}$. Fits are from the three-state relaxation model in Scheme 1, and the overlaid data points at 0.55 and 9.14 M urea are from double-jump experiments in panel E (Table S4). (E) Unfolding amplitudes of swap$^{\beta 2}$ at 9.14 M urea, after refolding has proceeded at 0.55 M urea for various delay times. The two unfolding amplitudes (red and blue) were obtained from a double-exponential fit of the unfolding time course, yielding rate constants matching those of P$^{2/3n}$ and P$^{1/2}$ (red and blue squares in panel D). The amplitudes display two phases. First is a fast growth with rate constants that superimpose with the first refolding phase of the swap$^{\beta 2}$ chevron plot (red ×^{1st} and blue +^{1st} in panel D). Second is a slower re-equilibration with rate constants that match the second refolding phase of the swap$^{\beta 2}$ chevron plot (red ×^{2nd} and blue +^{2nd} in panel D). The population changes follow precisely the stabilities of the references P$^{2/3n}$ and P$^{1/2}$. Displayed global fits are from the three-state relaxation in Scheme 1, and the double-jump relaxation rate constants in panel E (×, +) were obtained by free double-exponential fits to the amplitudes vs delay time data.

Table 1. Kinetic Parameters for the Swap Constructs Derived from Data in Figures 2–4, According to Eqs S5 and S6, and for the Permutant References Derived According to Eq S1[a]

	log k_f^{A,H_2O}	m_f^A	log k_u^{A,H_2O}	m_u^A	log k_f^{B,H_2O}	m_f^B	log k_u^{B,H_2O}	m_u^B
swap$^{\beta 2}$	−1.34 ± 0.86	−0.97 ± 1.23	−2.69 ± 0.44	0.23 ± 0.07	−1.34 ± 0.82	−0.97 ± 1.23	−3.30 ± 0.41	0.23 ± 0.07
P$^{2/3n}$	−1.30 ± 0.05	−0.96 ± 0.06	−2.93 ± 0.03	0.30 ± 0.01				
P$^{1/2}$					−1.20 ± 0.07	−0.97 ± 0.08	−3.43 ± 0.05	0.24 ± 0.08
swap$^{\beta 3}$	−0.53 ± 0.97	−0.91 ± 1.36	−0.77 ± 0.38	0.38 ± 0.12	−1.36 ± 0.91	−0.91 ± 1.36	−3.05 ± 1.11	0.25 ± 0.01
P$^{3/4n}$	−0.16 ± 0.00	−1.15 ± 0.1[b]	−0.54 ± 0.04	0.41 ± 0.01				
P$^{2/3c}$					−1.08 ± 0.10	−1.15 ± 0.13	−3.05 ± 0.09	0.27 ± 0.03
swap$^{\beta 8}$	−0.36 ± 0.52	−0.88 ± 0.60	−2.60 ± 0.34	0.20 ± 0.07	−0.72 ± 0.48	−0.80 ± 0.50	−3.71 ± 0.40	0.25 ± 0.07
P$^{7/8c}$	−0.38 ± 0.03	−0.86 ± 0.02	−2.84 ± 0.02	0.23 ± 0.00				
P$^{8/1n}$					−0.51 ± 0.02	−0.87 ± 0.01	−3.88 ± 0.02	0.27 ± 0.00
swap$^{\beta 1-4}$	0.30 ± 0.88	−0.99 ± 0.43	−3.54 ± 0.42	0.50 ± 0.16	−0.40[c]	−0.85[c]	−3.60 ± 0.23	0.23 ± 0.06
P$^{4/5n}$	−0.11 ± 0.01	−0.79 ± 0.01	−3.26 ± 0.03	0.43 ± 0.01				
P$^{8/1c}$					−0.40 ± 0.02	−0.85 ± 0.01	−3.74 ± 0.03	0.25 ± 0.00
swap$^{\beta 5-8}$	0.17 ± 0.02	−0.88 ± 0.01	−2.78 ± 0.02	0.45 ± 0.01	−1.29 ± 0.05	−0.63 ± 0.02	−3.87 ± 0.02	0.28 ± 0.00
P$^{4/5c}$	−0.04 ± 0.05	−0.80 ± 0.04	−2.86 ± 0.06	0.44 ± 0.01				
P$^{8/1n}$					−0.51 ± 0.02	−0.87 ± 0.01	−3.88 ± 0.02	0.27 ± 0.00

[a]Rate constants are in units of s^{-1}, and m values in units of M^{-1}. [b]Locked to m_f of P$^{2/3c}$ because of the low transition midpoint of P$^{3/4n}$ (Figure 3). [c]Locked to values of P$^{8/1c}$ due to amplitude cancellation of the slow refolding limb of swap$^{\beta 1-4}$, cf. Figure 4 and Figure S10.

constructs swap$^{\beta 2}$, swap$^{\beta 3}$, and swap$^{\beta 8}$ exhibit clean HSQC spectra fully analogous to those of the reference structures P$^{1/2}$, P$^{2/3}$, and P$^{1/8}$ (Figure S4). Consistently, swap$^{\beta 2}$/P$^{1/2}$, swap$^{\beta 3}$/P$^{2/3}$, and swap$^{\beta 8}$/P$^{1/8}$ are also predicted to be the dominating ground-state structures at 0 M urea, according to their thermodynamic stabilities (Figures 2 and 3, Table 1). Upon urea titration, these ground states display cooperative unfolding transitions (Figure S5), matching those of the references P$^{1/2}$, P$^{2/3c}$,

DOI: 10.1021/jacs.6b05151
J. Am. Chem. Soc. 2016, 138, 15571−15579

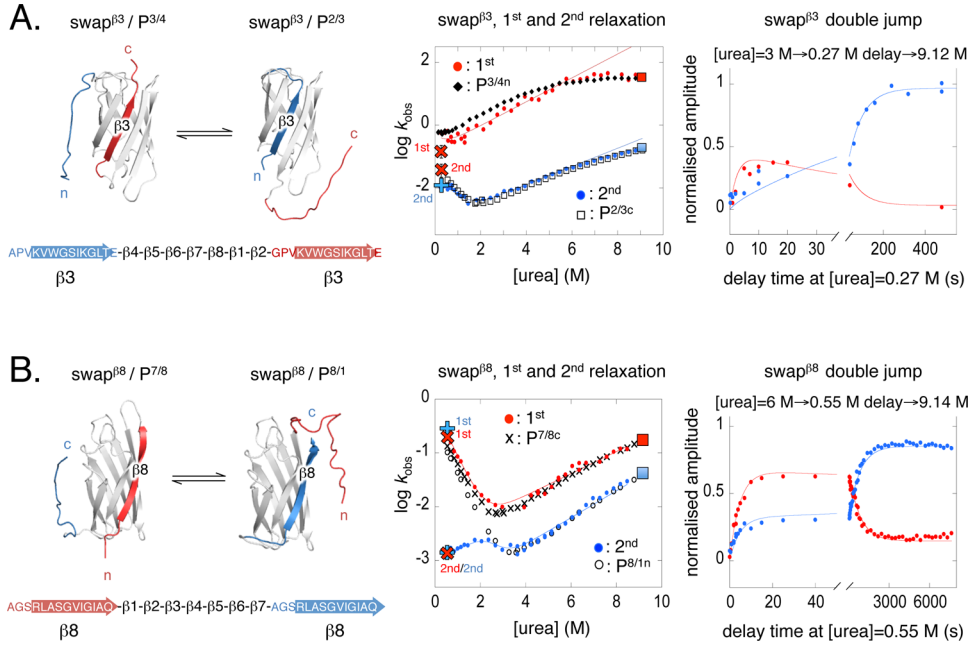

Figure 3. Structures and folding behavior of swap$^{\beta 3}$ and swap$^{\beta 8}$. (A) Left: Structures of the competing states of swap$^{\beta 3}$ based on the permutant references $P^{3/4}$ (inferred from PDB 5J0F) and $P^{2/3}$ (PDB 5J0C). Middle: Biphasic chevron plot of swap$^{\beta 3}$ superimposed with those of the permutant references $P^{3/4n}$ and $P^{2/3c}$. Fits are from the three-state relaxation model in Scheme 1, and the overlaid data points at 0.27 and 9.12 M urea are from the double-jump experiments in the right panel (Table S4). Right: Amplitude vs delay time plot used to obtain the overlaid relaxation rate constants in the chevron panel (red ×$^{1st/2nd}$ and blue +^{2nd}). As the rapid relaxation of the amplitudes from the second unfolding phase is undefined, the rate constant +^{first} is missing in the chevron panel. The amplitudes from the first unfolding phase cannot be accurately determined above 100 s delay times in the double-jump mode due to amplitude domination from the second unfolding phase. Accordingly, the single data point at 480 s has been obtained by standard stopped-flow mixing of 0.27 → 9.12 M urea, where the signal-to-noise is better (Figure S5). Displayed global fits are from the three-state relaxation in Scheme 1. Fits of log k_u are extended beyond the transition region to clarify extrapolations to 0 M urea; i.e., the change of rate-limiting step ‡′ → ‡″ at high [urea] is not included in the extrapolation. (B) Left: Structures of the competing states of swap$^{\beta 8}$ based on the permutant references $P^{7/8}$ (PDB 5J0G) and $P^{8/1}$ (PDB 4BCZ). Middle and right: Data panels are as described in (A), with the difference that all four relaxation rate constants (red ×$^{1st/2nd}$ and blue +$^{1st/2nd}$) are well defined by the double-jump data. Displayed global fits are from the three-state relaxation in Scheme 1.

and $P^{1/8n}$ (Figures 2 and 3, Table 1, and Table S2). The HSQC spectra of the "multi-strand" constructs swap$^{\beta 1-4}$ and swap$^{\beta 5-8}$, on the other hand, show perfect mixtures of the states swap$^{\beta 1-4}$/$P^{8/1}$, swap$^{\beta 1-4}$/$P^{4/5}$, swap$^{\beta 5-8}$/$P^{8/1}$, and swap$^{\beta 5-8}$/$P^{4/5}$ (Figure S5). Again, the results are fully consistent with the thermodynamic stabilities of their references states at 0 M urea (Figure 4, Table 1), and urea titration yields unfolding transitions corresponding to those of $P^{4/5n}$, $P^{1/8c}$, $P^{4/5c}$, and $P^{1/8n}$ (Figure S5, Table S2). Finally, the HSQC data verify that the un-recruited β-strand copies protrude disordered from the strand-swap constructs; i.e., the non-overlapping cross peaks display archetypically disordered signal by being clustered at the central parts of the spectra (Figure S6).

Strand-Swap Kinetics. For ease of analysis, the ideal strand-swap construct is one that first folds up with one copy of the target β-strand and, once the native state is formed, swaps to the other. Such behavior is illustrated by the example swap$^{\beta 2}$ construct in Figure 2. Upon dilution of urea-denatured swap$^{\beta 2}$ into stabilizing conditions at [urea] = 0.55 M, the protein displays first a fast refolding phase with rate constant $k_f^{fast} = 0.029\ s^{-1}$, followed by a slower re-equilibration phase with rate constant $k_f^{slow} = 0.0017\ s^{-1}$ (Figure 2). The fast phase matches well the refolding rate constant (k_f) of the reference permutant $P^{2/3n}$ (Figure 2, Table S1). In contrast, the k_f^{slow} phase is unique for swap$^{\beta 2}$ by being slower than k_f for the alternate reference $P^{1/2}$. At [urea] > 1 M, however, the values of k_f^{slow} and the kinetics of $P^{1/2}$ converge (Figure 2). The rollover of log k_f^{slow} at low [urea] signals also that the relaxation is rate limited by an unfolding event.[21] It is thus reasonable to assume that the k_f^{slow} rollover is linked to the anticipated strand-swap conversion swap$^{\beta 2}$/$P^{2/3}$ → swap$^{\beta 2}$/$P^{1/2}$. To test this assumption, we used refolding−delay−unfolding experiments. In essence, fully denatured swap$^{\beta 2}$ was first mixed into stabilizing conditions at 0.55 M urea, and then folding was allowed to proceed for time t^{delay}, and finally the protein was jumped back to denaturing conditions at 9.14 M urea for analysis of unfolding rate constants and amplitudes (Figure 2). The experiments reveal unfolding of two species with rate constants matching those of $P^{2/3n}$ and $P^{1/2}$ (Figure 2, Table 1). Upon plotting the amplitudes of these unfolding phases vs t^{delay}, we observe in turn two relaxation events (Figure 2). First is a parallel amplitude growth matching k_f^{fast}, followed by a slower amplitude re-equilibration matching k_f^{slow}. If this slow re-equilibration corresponds to the swap$^{\beta 2}$/$P^{2/3}$ → swap$^{\beta 2}$/$P^{1/2}$ relaxation, the $\beta 2$ exchange does not take place rapidly in the native basin. Rather, it seems enslaved to the global unfolding of $P^{2/3n}$ ($k_u = 0.0027\ s^{-1} \approx k_f^{slow}$, Table 1). To examine this possibility, we modeled the system with the minimal three-state process,

Scheme 1

$$N^A \underset{k_f^A}{\overset{k_u^A}{\rightleftharpoons}} D \underset{k_u^B}{\overset{k_f^B}{\rightleftharpoons}} N^B$$

where D is the denatured ensemble, N^A and N^B are the two alternative folded states, and k_f^A, k_f^B, k_u^A, and k_u^B are the associated refolding and unfolding rate constants. The characteristic relaxation rate constants of Scheme 1, i.e., k_{relax}^A and k_{relax}^B, are then given by

DOI: 10.1021/jacs.6b05151
J. Am. Chem. Soc. 2016, 138, 15571−15579

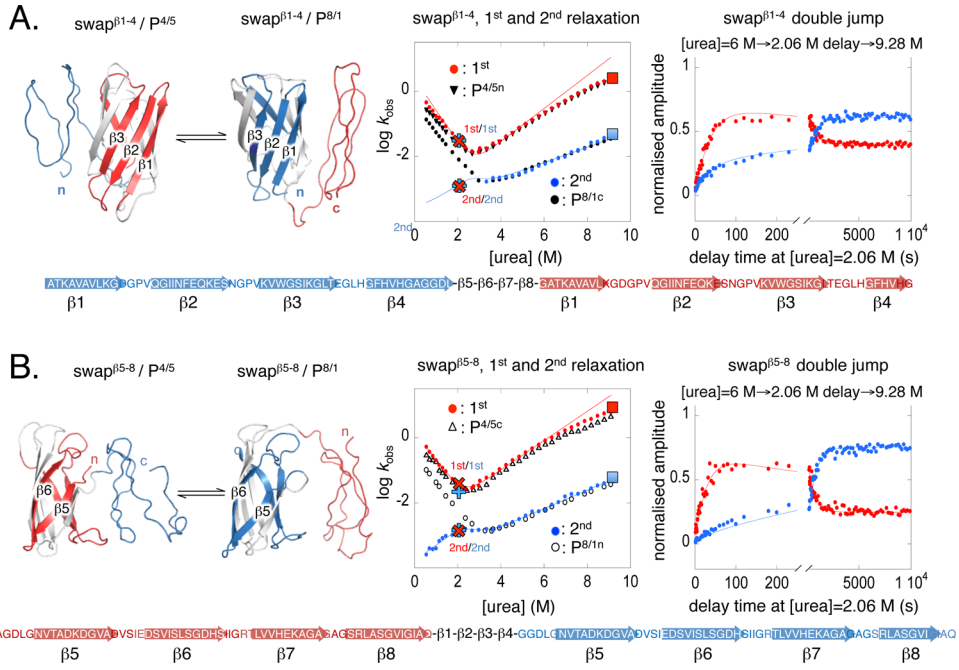

Figure 4. Structures and folding behavior of the multi-strand constructs swap$^{\beta1-\beta4}$ and swap$^{\beta5-\beta8}$. (A) Left: Structures of the competing states of swap$^{\beta1-\beta4}$ based on the permutant references $P^{4/5}$ (PDB 5J0F) and $P^{8/1}$ (PDB 4BCZ). Middle: Biphasic chevron plot of swap$^{\beta1-\beta4}$ superimposed with those of the permutant references $P^{4/5n}$ and $P^{8/1c}$. Fits are from the three-state relaxation model in Scheme 1, and the overlaid data points at 2.06 and 9.28 M urea are from the double-jump experiments in the right panel (Table S4). Right: Amplitude vs delay time plot used to obtain the overlaid relaxation rate constants in the chevron panel (red ×$^{1st/2nd}$ and blue +$^{1st/2nd}$). Displayed global fits are from the three-state relaxation in Scheme 1. Fits of log k_u are extended beyond the transition region to clarify extrapolations to 0 M urea. (B) Left: Structures of the competing states of swap$^{\beta5-\beta8}$ based on the permutant references $P^{4/5}$ (PDB 5J0F) and $P^{8/1}$ (PDB 4BCZ). Middle and right: Data panels are as described in (A).

$$k_{\text{relax}}^{\text{A,B}} = \frac{1}{2}\left(k_{\text{f}}^{\text{A}} + k_{\text{u}}^{\text{A}} + k_{\text{f}}^{\text{B}} + k_{\text{u}}^{\text{B}} \pm \sqrt{(k_{\text{f}}^{\text{A}} + k_{\text{u}}^{\text{A}} + k_{\text{f}}^{\text{B}} + k_{\text{u}}^{\text{B}})^2 - 4(k_{\text{u}}^{\text{A}}k_{\text{f}}^{\text{B}} + k_{\text{u}}^{\text{A}}k_{\text{u}}^{\text{B}} + k_{\text{u}}^{\text{B}}k_{\text{f}}^{\text{A}})}\right) \quad (1)$$

The expression is expanded in eqs S5 and S6 to include also the double-jump amplitudes and adapted to global fit of the data in Figures 2−4. As shown in Figure 2 and Table 1, the three-state model captures all aspects of the swap$^{\beta2}$ kinetics, without need to invoke further complexity: swap$^{\beta2}$ relaxes between the alternate states swap$^{\beta2}$/$P^{2/3}$ and swap$^{\beta2}$/$P^{1/2}$ via the denatured ensemble (Scheme 1). Also, the folding and re-equilibration of the swap$^{\beta2}$/$P^{2/3}$ and swap$^{\beta2}$/$P^{1/2}$ match well the kinetics of the references $P^{2/3n}$ and $P^{1/2}$. On this basis, we conclude that the exchange of $\beta2$ in the SOD1$^{\text{barrel}}$ does not occur locally but relies on global unfolding followed by global refolding (Figure 5). With reference to the macroscopic dynamics in Figure 1, the $\beta2$ segment seems thus prevented from local exchange on the native side of the unfolding barrier.

Moving the Analysis across the Entire SOD$^{\text{barrel}}$ Structure. Following the procedures above, we examined next the swap behavior of the single strands $\beta3$ and $\beta8$ (Figure 3, Table 1). Of interest is that $\beta2$,[22] $\beta3$,[18] and $\beta8$[19] have been implicated as key amyloidogenic segments of the SOD1 sequence and, thus, can put the protein at risk of aggregation if exposed transiently in the native basin.[16,19,23] In this regard, the c-terminal $\beta8$ stands out as especially vulnerable to native-state fraying,[16] as it partly lacks side-chain interactions in the unfolding transition state (‡″, Figure 6). Even so, the results show that the swap$^{\beta3}$ and swap$^{\beta8}$ constructs behave just as swap$^{\beta2}$ (Figure 3, Table 1): the kinetics follow the three-state relaxation in Scheme 1, which indicates that the exchange of $\beta3$ and $\beta8$ occurs via global unfolding. Notably, the relatively different refolding rate constants and stabilities of the competing states swap$^{\beta3}$/$P^{3/4}$ and swap$^{\beta3}$/$P^{2/3}$ lead to heavily biased populations in the two relaxation steps. This bias makes the double-jump amplitudes of the minor state swap$^{\beta3}$/$P^{3/4}$ difficult to determine with accuracy (Figure 3). It is nevertheless clear that accumulation of swap$^{\beta3}$/$P^{3/4}$ dominates the first phase and accumulation of swap$^{\beta3}$/$P^{2/3}$ the second phase. The just fractional occupancy of ∼0.4 for swap$^{\beta3}$/$P^{3/4}$ around t^{delay} = 5 s is due to this species being close to the transition midpoint under the delay conditions at 0.27 M urea and thus coexisting with fully denatured protein. Although the relaxation rate constants from double-jump of swap$^{\beta3}$ have larger errors than the other constructs, it is evident that the second amplitude relaxation is considerable slower than k_u of swap$^{\beta3}$/$P^{3/4}$, as predicted for $\beta3$ exchange via global unfolding (Scheme 1, Figure 5, and Figure S7). To investigate also the behavior of the remaining strands $\beta4$ and $\beta5$, we moved on to analyze the swap$^{\beta4}$ and swap$^{\beta5}$ constructs. These strands are implicated in allosteric control and seen to display tunable dynamics by NMR.[10] Because of the low stabilities of the swap$^{\beta4}$/$P^{3/4}$ and swap$^{\beta5}$/$P^{5/6}$ species, however, they did not sufficiently populate to allow stopped-flow detection (Figure S8). The inability to directly target the $\beta4$ and $\beta5$ kinetics prompted us instead to determine how these strands interact in the unfolding transition state of the SOD1$^{\text{barrel}}$ by phi-value analysis (see Clues from Transition-State Structure, below).

Multi-strand Swaps. The question is then, what happens upon insertion of multiple strands to swap? Such design not only enables analysis of contiguous regions of the SOD1$^{\text{barrel}}$ structure, such as those implicated in partly ruptured intermediates,[24] but also opens up for *intermolecular* formation of more complex aggregation nuclei.[25] To cover as many outcomes as possible, we

DOI: 10.1021/jacs.6b05151
J. Am. Chem. Soc. 2016, 138, 15571−15579

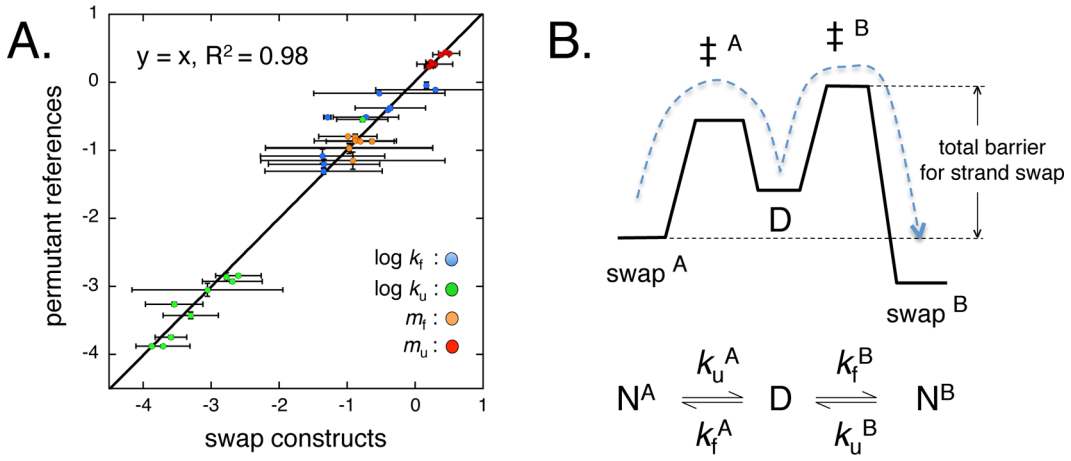

Figure 5. Model-free control. (A) Folding kinetics of the strand-swap constructs vs the permutant reference structures (data from Table 1). The *y*-axis displays the kinetic parameters for the strand-swap constructs derived from fit of eqs S5 and S6, and the *x*-axis the corresponding parameters for the permutant references derived from fit of eq S1. The plot shows that the biphasic relaxations of the strand-swap constructs match well the two-state transitions of the permutant references (Figures 2–4), providing independent evidence that β-strand swap follows global unfolding: folding of the strand-swap constructs is the sum of two cooperative transitions according to Scheme 1. (B) The corresponding free-energy profile is the combination of two competing two-state transitions, linked via a common denatured state. Blue arrow indicates the relaxation pathway of species $swap^A$ to $swap^B$, with the effective exchange barrier given by the free-energy difference between $swap^A$ and $‡^B$. The associated deviation between the rate constants for $swap^A$ unfolding and β-strand exchange is particularly notable for $swap^{\beta 3}$ in Figure 3.

opted for constructs with the maximum number of exchangeable strands, i.e., four out of eight (Figure 4). The combinatorial outcome of four exchangeable strands is five competing permutant states (Figure S9). The constructs were aimed to probe—as selectively as possible—the swap behavior of barrel regions that become structured early and late in the SOD1 folding process.[16] These early and late regions are indicated by the distributions of high and low phi-values[16] in the SOD1 transition states (‡′ and ‡″, Figures 1 and 6). The designs that best fulfill these criteria are (i) $swap^{\beta 1-4}$, which targets the major part of the high phi-value nucleus, and (ii) $swap^{\beta 5-8}$, which entails mainly the peripheral low phi-value regions that fold late (Figure 6). Despite their complexity, the multi-strand constructs behave as cooperatively and predictably as the single-strand dittos: both $swap^{\beta 1-4}$ and $swap^{\beta 5-8}$ display predominantly three-state relaxations involving the two most stable ground-state structures, $P^{4/5}$ and $P^{8/1}$ (Figure 4). The slow refolding phase of $swap^{\beta 1-4}$ becomes invisible at low [urea] due to amplitude cancellation but re-emerges predictably upon changing denaturant to GdmCl (Figure S10). Contributions from the other competing structures, i.e., $P^{7/8}$, can be discerned for $swap^{\beta 5-8}$ upon extending the fitting model to >3 states but are small in accordance with their relatively low stabilities (Figure S10). The cooperative behavior of $swap^{\beta 1-4}$ and $swap^{\beta 5-8}$ adheres thus with earlier observations of global unfolding in complete domain-swap.[26] Somewhat surprisingly, we find no indication of transient aggregation,[27] misfolding,[21] or intermolecular domain swap[28] in the stopped-flow experiments (Figure S11), as recently observed with tandem repeats of titin.[29] The possible exception is a tendency of $swap^{\beta 1-4}$ to transiently dimerize during purification (sometimes visual in gels) that we tentatively assign to intermolecular domain swapping. However, this dimerization is not identified by varying protein concentration in the stopped-flow analysis (Figure S11), suggesting either that the accumulation is small or that the kinetics involved overlap with the strand-swap events.

Additional Controls of the Three-State Relaxation Behavior. To further test the Scheme 1 mechanism, we performed a series of mutational controls on $swap^{\beta 1-4}$. First, we eradicated the individual of the $swap^{\beta 1-4}$ relaxation phases by Trp mutation. As predicted from the results in Figures 2–4, the mutation W146A, targeting selectively the species $swap^{\beta 1-4}/P^{4/5}$, leaves only the phases for the competing state $swap^{\beta 1-4}/P^{8/1}$ (Figure S12). *Vice versa*, the mutation W32A leaves only the phases for $swap^{\beta 1-4}/P^{4/5}$ (Figure S12). Second, we selectively perturbed $swap^{\beta 1-4}/P^{8/1}$ by the severely destabilizing mutation I35A. The mutation reduces the kinetics to a single chevron plot, identical to that of the alternate state $P^{4/5n}$ (Figure S12), and shifts the ground-state equilibrium entirely to $swap^{\beta 1-4}/P^{4/5}$, as detected by HSQC NMR (Figure S13). Again, the data show full agreement with the minimal three-state relaxation in Scheme 1, the thermodynamic stabilities in Table 1, and equilibrium unfolding data (Figure S5). To finally validate that the constructs undergo β-strand exchange in a fully cooperative manner, as indicated by the kinetics in Figures 2–4, we mapped out the urea equilibrium transition for $swap^{\beta 1-4}$ by HSQC NMR and double-jump mixing (Figure S14). The results show that even this extreme construct, involving four exchangeable strands and five competing states (Figure S9), displays a clean cooperative transition between the most stable structures, $swap^{\beta 1-4}/P^{4/5}$ and $swap^{\beta 1-4}/P^{8/1}$ (Figure S6). Moreover, the urea dependence of this structural shift matches the *m*-value difference between the reference states $P^{4/5n}$ and $P^{8/1c}$, providing direct thermodynamic support for the mechanism in Scheme 1 (Table 1, Figure S14).

Model-Free Control. As last control we plotted simply the kinetic parameters obtained for the biphasic strand-swap constructs in Figures 2–4 versus those of the reference permutants. Data yield a linear correlation with $R^2 = 0.98$ (Figure 5), suggesting that the strand-swap constructs are kinetically the combinations of their reference permutants. The folding free-energy profiles of the strand-swap constructs are well described by the sum of two cooperative transitions linked by a common denatured ensemble (Figure 5).

Clues from Transition-State Structure. To examine why the $SOD1^{barrel}$ needs to traverse the entire unfolding barrier to swap strands, we looked into the structures of the unfolding transition states with phi-value analysis.[11] From the curved chevron

DOI: 10.1021/jacs.6b05151
J. Am. Chem. Soc. 2016, 138, 15571–15579

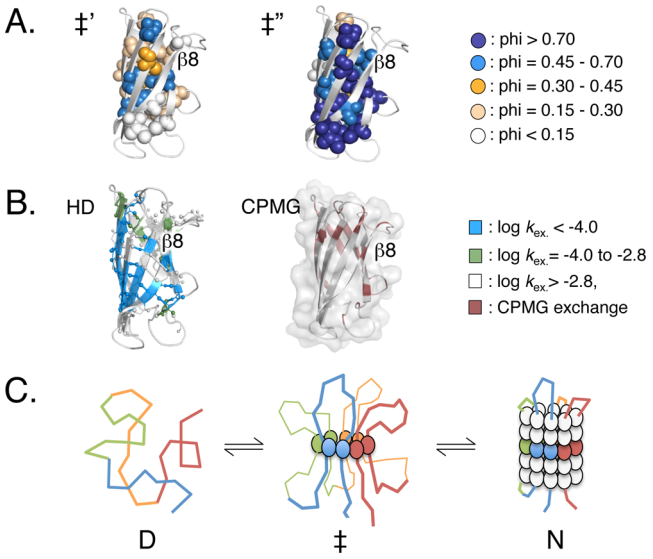

Figure 6. Transition-state structure, native-state dynamics, and implicated folding mechanism of SOD1^{barrel}. (A) The interactions of the early (‡′) and late (‡″) transition states of SOD1^{barrel} as determined by phi-value analysis (SI). Upon folding ‡′ → ‡″, the interactions expand to encompass most parts of the β-barrel structure. (B) The H−D exchange kinetics of SOD1^{barrel} shows a contiguous pattern of protected backbone amides that involves the majority of the barrel β strands. The strand with the weakest protection is β5 (adapted from data in ref 10). Similarly, NMR CPMG analysis indicates breathing motions that overall comply with the phi-value and H−D exchange data but reveals also local motions in other directions of the native-state basin (adapted from data in ref 10). (C) Model for in-register alignment of β-strands during folding. The schematic depiction shows the extreme case where the radial folding nucleus[16,33] is confined to a single layer of core residues. "D" is the denatured ensemble, "‡" is the transition state, and "N" is the native state. In the early transition state of SOD1^{barrel} (‡′, panel A), the corresponding layer is less well-defined and partly open, but the mechanism presents still a consistent explanation to why β-strand swap requires the protein to globally unfold (Figures 2−4).

data in Figure 2, it is apparent that the protein undergoes a Hammond shift[30] from an early (‡′) to a late (‡″) barrier maximum at high [denaturant] (Figure 1). Following the approach applied to U1A[31] and S6,[32] the ‡′ and ‡″ phi-values were obtained from urea and GdmCl data, respectively (SI, including Figure S15). The key motivation for this hybrid approach is that urea allows the refolding kinetics and ‡′ to be measured accurately for severely destabilized mutants, whereas GdmCl is required for shifting the unfolding kinetics into the "curved" ‡″ regime (Figure 2). The results are presented in Figure 6 and Table S3. Similar to what has been observed for the wild-type apoSOD1 monomer,[16] we find that the highest phi values of ‡′ tend to form a layer across the SOD1^{barrel} core (Figure 6). Even though a general decrease of phi-values in SOD1^{barrel} diffuses this layered pattern relative to the wild-type apoSOD1 monomer (Figure S16), the folding nucleus seems on the whole to capture and align the β-strands "by their waists" (Figure 6). The exceptions are β5 and β8 that maintain phi values of approximately zero in the early transition state ‡′ (Table S3). This disc-like arrangement of the folding nucleus is not unique for SOD1, but is also observed for the β-barrel protein TNfn3.[33] Upon progressing to the late transition state ‡″ the side-chain contacts seem to consolidate further and expand spatially to integrate also β5 (phi > 0.45) and β8 (phi > 0.70) (Figure 6, Table S3). Although the phi-values probe only the side-chain interactions, they point to a picture where all strands of the SOD1^{barrel} are tied in to the folding nucleus at the top of the unfolding barrier ‡″. Matching patterns of cross-strand interactions emerge also at the lower levels of the native basin, as indicated by H−D exchange analysis[14] and CPMG NMR.[10] The globally exchanging amide groups of SOD1^{barrel} outlines a contiguous linkage of stable hydrogen bonds that connects all strands, save β5, at the edge of the active-site sheet[14] (Figure 6). Consistently, β5 also stands out as dynamic at the very lowest levels of the native basin as measured by CPMG relaxation analysis[10] (Figure 6). The only evidence that swapping of this edge strand occurs by global unfolding is thus from phi-value data of the late transition state ‡″ (Figure 6), which previously went unnoticed in analysis of the wild-type apoSOD1 monomer.[16] Since phi-values and dynamic motions need not to be linked in systems with parallel unfolding pathways, however, we consider this evidence alone as inconclusive.[13] Even so, the combined data in Figures 2−6 leave us with a coherent picture of the strand-swap events from bottom to top of the unfolding barrier in Figure 1: the SOD1^{barrel} chain seems fixed by a belt of tertiary bonds that encompasses the entire perimeter of the β-barrel, with the possible exception of β5 at the edge of the active-site sheet.

DISCUSSION

Folded-State Behavior and Implications for SOD1 Aggregation. In light of the extensive sequence alterations made to the various strand-swap constructs in this study (Figures 2−4), their structural behavior stands out as remarkably uniform and robust: dislodgement and re-insertion of individual β-strand segments in the SOD1 barrel do not take place locally but follow complete cycles of global unfolding and refolding (Figure 5). The chief ambiguity is here β4 and β5 of the active-site sheet, where low populations of transiently swapped species prevent conclusive analysis (Figure S8). Even so, when it comes to our question about conceivable precursors for aggregation, it seems unlikely that these are intermediates in the form of locally unfolded barrels. The SOD1 segments identified in aggregate structures, i.e., primarily β2, β3, and β8,[18,19,22] appear protected as long as the protein is on the native side of the folding barrier. In addition, the β2 and β3 segments will experience additional restriction in the disease-associated wild-type context where they reside anchored at either end, rather than just n- or c-terminally as in the strand-swap constructs (Figure 3). The results clarify thus at the structural level why the aggregation kinetics of mutant SOD1 *in vitro*, as well as survival times of transgenic ALS mice, correlate with the levels of globally unfolded protein:[7] the aggregation-competent epitopes of the SOD1 sequence are only free to interact intermolecularly upon complete rupture of the protective β-barrel (Figure 5). Notably, this interpretation challenges reports where SOD1 aggregation is traced to intermediates,[23,24] including our previous suggestion that aggregation-prone strands are exposed by native-state fraying.[16] From the perspective of identifying targets for disease intervention,[6] it is pressing to clarify whether these conflicting interpretations stem from variable sample conditions, heterogeneous protein material or, like in our seminal SOD1 phi analysis,[16] lacking access to the decisive control.

Implications for Folding. The global strand-swap behavior sheds also new detail on the mechanism of β-barrel folding. Generally, the structural repertoire of folded proteins is determined by the free-energy landscape of the native side of the folding barrier, i.e., the native basin.[34,35] Imperceptible from the macroscopic projection in Figure 1, this microscopic native

DOI: 10.1021/jacs.6b05151
J. Am. Chem. Soc. 2016, 138, 15571−15579

basin is multi-dimensional and allows dynamic motions in all directions that are energetically accessible.[36] The unfolding pathway that is ultimately controlled by the most favorable route for barrier crossing (‡) needs thus not to follow the most prevalent ground-state dynamics.[13] Although the present data are not conclusive regarding this specific issue, it is possible that the slight mismatches between the phi-values and H−D exchange patterns in Figure 6 relate to such decoupling between the unfolding pathway and the ground-state dynamics. Another notable detail is that the rate constants for strand swap (k_{relax}^{B} = 10^{-4}–10^{-2} s^{-1}, Figures 2–4) match closely those of monomer dissociation from β-pleated fibrils, $k_{diss} \approx 10^{-4}$ s^{-1}.[37,38] Similarly slow, erroneously paired β-strands of titin repeats are reported to interconvert with fully denatured species in the folding pre-equilibrium on a seconds time scale.[29] If such slow dissociation of de-solvated β-strand interfaces is universal, then folding pathways relying on strand-register changes will be kinetically futile; i.e., the reconfiguration times[39] for opening and reclosing misfolded β-sheets (seconds) will end up in excessively long barrier-passage times.[40] A clue to how SOD1 evades such out-of-register traps is hinted by the phi-values. Similar to TNfn3,[33] the early transition-state of SOD1 (‡′) is overall biased to a layer of side-chain contacts that aligns the β-strand segments radially across an embryonic hydrophobic core (Figure 6). Upon progressing to the late transition state (‡″), this layer then seems to consolidate and expand axially to include also the bottom and top parts of the SOD1 barrel. Assuming that these core interactions are accompanied by de-solvation[41] and backbone hydrogen bonding,[42] we arrive at a picture where the successful nucleus aligns, from the very beginning, the β-strands in correct register and thus dodges the slow shuffling dynamics. This, of course, does not exclude that the protein attempts to fold also via out-of-register excitations, but these will be kinetically penalized by increased reconfiguration times, i.e., local trapping.[43] The interpretation highlights the influence of conformation-dependent reconfiguration times[39] in kinetic partitioning, provoking the question if β-sheet structures are generally biased to in-register transitions because the energetically viable alternatives are too slow? It also points to the possibility that low levels of trapped states will eventually emerge as "glassy"[44] debris across the free-energy landscape,[39] providing the protein is kept long enough at equilibrium. With SOD1, however, the population of such trapped species seems sparse *in vitro*. As discussed above, intermediate SOD1 species are also unlikely to present the principal precursors for *in vitro* aggregate growth, since this kinetically peaks at high concentrations of urea where the protein is globally unfolded.[45]

■ ASSOCIATED CONTENT

Supporting Information

The Supporting Information is available free of charge on the ACS Publications website at DOI: 10.1021/jacs.6b05151.

Additional figures and detailed method descriptions, including eqs S1–S10, Tables S1–S5, and Figures S1–S16 (PDF)

■ AUTHOR INFORMATION

Corresponding Author

*mikael@dbb.su.se

Notes

The authors declare no competing financial interest.

■ ACKNOWLEDGMENTS

Support was from the Swedish Research Council, Hjärnfonden, The Knut and Alice Wallenberg, Magnus Bergwall, and Bertil Hållsten foundations. We thank Pema Choden Bhutia for help with the phi-value analysis and sample preparations. Access to research infrastructure via BioNMR (Project 261863) is acknowledged. We also thank Martin Högbom group and Pål Stenmark group for help with crystallization.

■ REFERENCES

(1) Danielsson, J.; Mu, X.; Lang, L.; Wang, H.; Binolfi, A.; Theillet, F. X.; Bekei, B.; Logan, D. T.; Selenko, P.; Wennerstrom, H.; Oliveberg, M. *Proc. Natl. Acad. Sci. U. S. A.* **2015**, *112*, 12402.

(2) Smith, A. E.; Zhou, L. Z.; Gorensek, A. H.; Senske, M.; Pielak, G. J. *Proc. Natl. Acad. Sci. U. S. A.* **2016**, *113*, 1725.

(3) Wirth, A. J.; Gruebele, M. *BioEssays* **2013**, *35*, 984.

(4) Ferguson, N.; Becker, J.; Tidow, H.; Tremmel, S.; Sharpe, T. D.; Krause, G.; Flinders, J.; Petrovich, M.; Berriman, J.; Oschkinat, H.; Fersht, A. R. *Proc. Natl. Acad. Sci. U. S. A.* **2006**, *103*, 16248.

(5) Ciryam, P.; Tartaglia, G. G.; Morimoto, R. I.; Dobson, C. M.; Vendruscolo, M. *Cell Rep.* **2013**, *5*, 781.

(6) Walsh, D. M.; Selkoe, D. J. *Nat. Rev. Neurosci.* **2016**, *17*, 251.

(7) Lang, L.; Zetterstrom, P.; Brannstrom, T.; Marklund, S. L.; Danielsson, J.; Oliveberg, M. *Proc. Natl. Acad. Sci. U. S. A.* **2015**, *112*, 9878.

(8) Vallurupalli, P.; Hansen, D. F.; Kay, L. E. *Proc. Natl. Acad. Sci. U. S. A.* **2008**, *105*, 11766.

(9) Bai, Y.; Sosnick, T. R.; Mayne, L.; Englander, S. W. *Science* **1995**, *269*, 192.

(10) Danielsson, J.; Awad, W.; Saraboji, K.; Kurnik, M.; Lang, L.; Leinartaite, L.; Marklund, S. L.; Logan, D. T.; Oliveberg, M. *Proc. Natl. Acad. Sci. U. S. A.* **2013**, *110*, 3829.

(11) Matouschek, A.; Kellis, J. T., Jr.; Serrano, L.; Fersht, A. R. *Nature* **1989**, *340*, 122.

(12) Lindberg, M. O.; Oliveberg, M. *Curr. Opin. Struct. Biol.* **2007**, *17*, 21.

(13) Haglund, E.; Lind, J.; Oman, T.; Ohman, A.; Maler, L.; Oliveberg, M. *Proc. Natl. Acad. Sci. U. S. A.* **2009**, *106*, 21619.

(14) Danielsson, J.; Kurnik, M.; Lang, L.; Oliveberg, M. *J. Biol. Chem.* **2011**, *286*, 33070.

(15) Khare, S. D.; Dokholyan, N. V. *Proc. Natl. Acad. Sci. U. S. A.* **2006**, *103*, 3147.

(16) Nordlund, A.; Oliveberg, M. *Proc. Natl. Acad. Sci. U. S. A.* **2006**, *103*, 10218.

(17) Nordlund, A.; Leinartaite, L.; Saraboji, K.; Aisenbrey, C.; Grobner, G.; Zetterstrom, P.; Danielsson, J.; Logan, D. T.; Oliveberg, M. *Proc. Natl. Acad. Sci. U. S. A.* **2009**, *106*, 9667.

(18) Bergh, J.; Zetterstrom, P.; Andersen, P. M.; Brannstrom, T.; Graffmo, K. S.; Jonsson, P. A.; Lang, L.; Danielsson, J.; Oliveberg, M.; Marklund, S. L. *Proc. Natl. Acad. Sci. U. S. A.* **2015**, *112*, 4489.

(19) Ivanova, M. I.; Sievers, S. A.; Guenther, E. L.; Johnson, L. M.; Winkler, D. D.; Galaleldeen, A.; Sawaya, M. R.; Hart, P. J.; Eisenberg, D. S. *Proc. Natl. Acad. Sci. U. S. A.* **2014**, *111*, 197.

(20) Haglund, E.; Lindberg, M. O.; Oliveberg, M. *J. Biol. Chem.* **2008**, *283*, 27904.

(21) Otzen, D. E.; Oliveberg, M. *Proc. Natl. Acad. Sci. U. S. A.* **1999**, *96*, 11746.

(22) Oliveberg, M. *Nat. Methods* **2010**, *7*, 187.

(23) Ding, F.; Furukawa, Y.; Nukina, N.; Dokholyan, N. V. *J. Mol. Biol.* **2012**, *421*, 548.

(24) Banci, L.; Bertini, I.; Boca, M.; Calderone, V.; Cantini, F.; Girotto, S.; Vieru, M. *Proc. Natl. Acad. Sci. U. S. A.* **2009**, *106*, 6980.

(25) Zheng, W.; Schafer, N. P.; Wolynes, P. G. *Proc. Natl. Acad. Sci. U. S. A.* **2013**, *110*, 1680.

(26) Liu, L.; Byeon, I. J.; Bahar, I.; Gronenborn, A. M. *J. Am. Chem. Soc.* **2012**, *134*, 4229.

(27) Otzen, D. E.; Kristensen, O.; Oliveberg, M. *Proc. Natl. Acad. Sci. U. S. A.* **2000**, *97*, 9907.

DOI: 10.1021/jacs.6b05151
J. Am. Chem. Soc. 2016, 138, 15571–15579

(28) Silow, M.; Tan, Y. J.; Fersht, A. R.; Oliveberg, M. *Biochemistry* **1999**, *38*, 13006.
(29) Borgia, A.; Kemplen, K. R.; Borgia, M. B.; Soranno, A.; Shammas, S.; Wunderlich, B.; Nettels, D.; Best, R. B.; Clarke, J.; Schuler, B. *Nat. Commun.* **2015**, *6*, 8861.
(30) Oliveberg, M.; Tan, Y. J.; Silow, M.; Fersht, A. R. *J. Mol. Biol.* **1998**, *277*, 933.
(31) Ternstrom, T.; Mayor, U.; Akke, M.; Oliveberg, M. *Proc. Natl. Acad. Sci. U. S. A.* **1999**, *96*, 14854.
(32) Lindberg, M. O.; Haglund, E.; Hubner, I. A.; Shakhnovich, E. I.; Oliveberg, M. *Proc. Natl. Acad. Sci. U. S. A.* **2006**, *103*, 4083.
(33) Hamill, S. J.; Steward, A.; Clarke, J. *J. Mol. Biol.* **2000**, *297*, 165.
(34) Frauenfelder, H.; McMahon, B. H.; Austin, R. H.; Chu, K.; Groves, J. T. *Proc. Natl. Acad. Sci. U. S. A.* **2001**, *98*, 2370.
(35) Zhuravlev, P. I.; Hinczewski, M.; Chakrabarti, S.; Marqusee, S.; Thirumalai, D. *Proc. Natl. Acad. Sci. U. S. A.* **2016**, *113*, E715.
(36) Oliveberg, M.; Wolynes, P. G. *Q. Rev. Biophys.* **2005**, *38*, 245.
(37) Narayan, P.; Orte, A.; Clarke, R. W.; Bolognesi, B.; Hook, S.; Ganzinger, K. A.; Meehan, S.; Wilson, M. R.; Dobson, C. M.; Klenerman, D. *Nat. Struct. Mol. Biol.* **2012**, *19*, 79.
(38) Gruning, C. S.; Klinker, S.; Wolff, M.; Schneider, M.; Toksoz, K.; Klein, A. N.; Nagel-Steger, L.; Willbold, D.; Hoyer, W. *J. Biol. Chem.* **2013**, *288*, 37104.
(39) Bryngelson, J. D.; Onuchic, J. N.; Socci, N. D.; Wolynes, P. G. *Proteins: Struct., Funct., Genet.* **1995**, *21*, 167.
(40) Chung, H. S.; Eaton, W. A. *Nature* **2013**, *502*, 685.
(41) Fernandez-Escamilla, A. M.; Cheung, M. S.; Vega, M. C.; Wilmanns, M.; Onuchic, J. N.; Serrano, L. *Proc. Natl. Acad. Sci. U. S. A.* **2004**, *101*, 2834.
(42) Deechongkit, S.; Nguyen, H.; Powers, E. T.; Dawson, P. E.; Gruebele, M.; Kelly, J. W. *Nature* **2004**, *430*, 101.
(43) Chung, H. S.; Louis, J. M.; Eaton, W. A. *Proc. Natl. Acad. Sci. U. S. A.* **2009**, *106*, 11837.
(44) Bryngelson, J. D.; Wolynes, P. G. *Proc. Natl. Acad. Sci. U. S. A.* **1987**, *84*, 7524.
(45) Lang, L.; Kurnik, M.; Danielsson, J.; Oliveberg, M. *Proc. Natl. Acad. Sci. U. S. A.* **2012**, *109*, 17868.

DOI: 10.1021/jacs.6b05151
J. Am. Chem. Soc. 2016, 138, 15571−15579